

SystolicAttention: Fusing FlashAttention within a Single Systolic Array

Jiawei Lin
jiawei.lin@epfl.ch
EPFL
Lausanne, Switzerland

Yuanlong Li
yuanlong.li@epfl.ch
EPFL
Lausanne, Switzerland

Guokai Chen
guokai.chen@epfl.ch
EPFL
Lausanne, Switzerland

Thomas Bourgeat
thomas.bourgeat@epfl.ch
EPFL
Lausanne, Switzerland

Abstract

Transformer models rely heavily on scaled dot-product attention (SDPA), typically implemented using the FlashAttention algorithm. However, current systolic-array-based accelerators face significant challenges when executing FlashAttention. Systolic arrays achieve high utilization primarily for consecutive and large matrix multiplications, whereas FlashAttention requires frequent interleaving of matrix multiplications and softmax operations.

The frequent data swaps between matrix multiplications on the systolic array and softmax operations on external units result in low array utilization. Moreover, when these computations run concurrently, the softmax stage contends with matrix multiplication for register file and SRAM ports, further degrading performance.

To overcome these limitations, we propose FSA, an enhanced systolic array architecture that enables the FlashAttention algorithm to run entirely within a single systolic array—eliminating the need for external vector units. At the core of FSA is SystolicAttention, a novel scheduling algorithm that maps FlashAttention operations onto systolic arrays with fine-grained, element-wise overlap. This approach significantly improves array utilization while preserving the original floating-point operation order to maintain numerical stability.

We implement FSA in synthesizable RTL and evaluate its performance against state-of-the-art commercial accelerators. Our results show that FSA achieves $1.77\times$ and $4.83\times$ higher attention FLOPs/s utilization compared to AWS Neuron v2 and Google’s TPUv5e, respectively, with only 12% area overhead.

CCS Concepts: • Computer systems organization → Systolic arrays; • Hardware;

Keywords: Systolic Array, Flash Attention, Microarchitecture, Accelerators

1 Introduction

The rapid advancement of artificial intelligence, particularly in natural language processing and computer vision, has been largely driven by the success of transformer models [14, 20, 45], which have revolutionized applications ranging from language translation and text generation [38] to image recognition [34] and autonomous driving [15]. However, the computational demands of transformer models are enormous [44], requiring specialized hardware accelerators to achieve practical performance and energy efficiency. As these models continue to grow in size and complexity [31], the need for efficient hardware acceleration becomes increasingly critical. One of the key operations in transformer models is the *scaled dot-product attention* (SDPA), which is often implemented using the *FlashAttention* [19, 42] algorithm. FlashAttention reduces memory overhead by breaking the Q , K , and V matrices into small tiles and fusing matrix multiplication with online softmax computation.

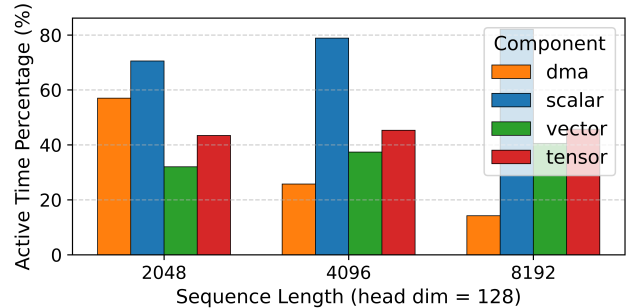


Figure 1. Active time percentage of different components in AWS NeuronCore-v2 when running FlashAttention.

Systolic arrays [35] are specialized hardware architectures that perform computation by streaming data through a network of tightly coupled processing elements (PEs). Many systolic array based accelerators with various dataflows [16, 17, 30, 37] have been proposed to accelerate deep learning workloads. In this paper, we focus on multiply-accumulate (MAC) based 2D systolic arrays, which are the most widely used

in commercial AI accelerators, such as Google’s TPU [23, 28, 29] and AWS NeuronCore [10]. In these architectures, data moves only one hop per clock cycle, minimizing hardware data movement overhead and enabling high scalability, which is crucial for efficiently executing large matrix multiplications.

When mapping FlashAttention to systolic array based accelerators, the matrix multiplication operations can be executed using the systolic array, while softmax-related operations must be offloaded to external vector and scalar units. To maximize hardware utilization, matrix multiplication and softmax operations from different iterations are often software-pipelined to run in parallel. Thus, the vector and scalar units must provide sufficient floating-point operations per second (FLOPs/s) to keep up with the systolic array. However, non-matrix-multiplication FLOPs/s are typically much lower in volume and more expensive to improve in hardware, resulting in a significant performance bottleneck. As shown in Figure 1, when running FlashAttention on AWS NeuronCore-v2, the systolic array (tensor engine) is only active for about 45% of the time, while the scalar unit remains active for 80% of the time.

Beyond the imbalance between matrix and non-matrix FLOPs/s, the complex data dependencies in FlashAttention also contribute to low systolic array utilization. Systolic arrays achieve high utilization when matrix data can be reused across multiple iterations, improving data locality and reducing the preloading overhead. However, in FlashAttention, the two matrix multiplications are separated by the softmax operation, preventing reuse of intermediate data. The softmax operation also causes frequent data transfers between the systolic array and the vector unit, further increasing preloading overhead and SRAM port contention [32, 49]. As shown in our experiments in subsection 6.1, the systolic array achieves less than 25% FLOPs/s utilization, even with 45% active time on AWS NeuronCore-v2, significantly lower than the theoretical peak FLOPs/s of the array.

The above problems can be addressed by executing the full FlashAttention algorithm entirely on the systolic array. In this case, non-matrix-multiplication operations can be computed using the matrix multiplication FLOPs/s available on the array itself. Additionally, data preloading overhead and SRAM port contention are eliminated since all computations occur within the same array. Achieving this, however, requires overcoming two key challenges. First, non-matrix-multiplication operations such as `exp`, `rowmax`, and `rowsum` must be efficiently implemented using only the systolic array. Second, different operations must be overlapped effectively to maximize utilization of the array.

COSA Plus [46] proposes mapping FlashAttention to two cooperative systolic arrays, but still requires the softmax operation to be performed by a special function unit (SFU), which may not provide sufficient FLOPs/s to keep up with the

systolic arrays. FuseMax [37] pioneered the fusion of FlashAttention into a single systolic array. It maps the `rowmax` and `rowsum` operations as spatial reductions and overlaps multiple FlashAttention iterations on the array simultaneously. However, it requires storing intermediate results using 10 registers per PE to support context switching between iterations, leading to additional register overhead.

We propose a new hardware-friendly systolic array architecture, **FSA**, which introduces minimal overhead to existing commercial systolic arrays and enables the execution of the full FlashAttention algorithm on a single systolic array. This design is guided by the following key insights: (1) the input values to the `exp` operation in FlashAttention are always less than or equal to zero. By splitting the input into integer and fractional parts, the fractional component falls within the range $(-1, 0]$, making it suitable for approximation via linear interpolation [33] reusing the MACs available on the systolic array; (2) the `rowmax` and `rowsum` operations can be expressed as reduction operations, which are well-supported in systolic architectures and can be performed on-the-fly as rows are generated in a streaming fashion; and (3) the operations within each FlashAttention iteration exhibit a dataflow pattern that allows fine-grained execution overlap, enabling multiple computations within the same iteration to proceed in parallel without waiting for the completion of prior steps. We also introduce **SystolicAttention**, a scheduling algorithm that makes the best use of FSA’s capabilities to overlap element-wise operations, significantly improving array utilization.

Our key contributions are as follows:

- We present FSA, an enhanced systolic array architecture capable of executing the full FlashAttention algorithm without relying on additional vector or scalar units. FSA is implemented in synthesizable RTL, requiring only 12% additional area compared to a standard design. The RTL implementation achieves a clock frequency of 1.5 GHz on a 16 nm process and 70 MHz on the Xilinx Alveo U55C FPGA.
- We demonstrate that all operations in FlashAttention can be element-wise overlapped on FSA using our proposed SystolicAttention scheduling algorithm. With SystolicAttention, FSA achieves 1.77× and 4.83× higher FLOPs/s utilization than AWS NeuronCore-v2 and TPUv5e, respectively, while preserving the original FlashAttention floating-point operation order for numerical stability.
- We develop a Python programming interface that enables users to write custom FSA kernels. Both the RTL implementation and the Python software stack are open-sourced at <https://github.com/VCA-EPFL/FSA>.

2 Background and Motivation

In this section, we first briefly introduce baseline systolic arrays and how they perform matrix multiplication. We then present the FlashAttention algorithm and discuss the challenges of implementing it on systolic array based accelerators. Finally, we elaborate on the insights and challenges of running the full FlashAttention algorithm entirely within a systolic array.

2.1 Systolic Array Architectures

Systolic arrays are a class of hardware accelerators that perform computations in a pipelined manner, where data flows through an array of processing elements (PEs) in a rhythmic fashion. Each PE performs a simple operation, such as a multiply-accumulate (MAC), and the data flows through the array in a wave-like pattern. Systolic arrays are particularly well-suited for matrix operations, such as matrix multiplication, as they can efficiently exploit data parallelism and locality. The dataflow of a systolic array defines how data moves through the array and the communication pattern between PEs. Common dataflows include *weight-stationary*, *input-stationary*, *output-stationary*, and *row-stationary* [16]. Due to the transpose rule of matrix products, weight-stationary and input-stationary dataflows can often be implemented using the same hardware. In this paper, we use the term *weight-stationary* to refer to both. As most deep learning workloads favor weight reuse, many systolic accelerators adopt the weight-stationary dataflow, such as Google’s TPU [23].

2.2 Matrix Multiplication on Systolic Arrays

An example weight-stationary systolic array is shown in Figure 2. It consists of $N \times N$ PEs, where each PE performs one floating-point MAC per cycle. One input matrix is tiled into $N \times N$ and preloaded into the array (*stationary matrix*). The other is tiled into $N \times M$ and streamed in from SRAM (*moving matrix*). The output is similarly tiled into $N \times M$ and streamed out.

Since the weight-stationary array does not retain the output matrix internally, output tiles are stored in a small, dedicated accumulation SRAM located at the bottom of the array. An accumulator unit reads values from this accumulation SRAM, combines the newly computed results from the systolic array with existing values, and writes the updated results back. This near-memory accumulation scheme is widely adopted in both open-source accelerators such as Gemmini [21], and commercial products such as AWS NeuronCore [10].

Preloading the stationary matrix requires N cycles at the start of computation. To ensure correctness, each row of the moving matrix must be delayed by 0 to $N - 1$ cycles before entering the array, and each column of the output matrix must be delayed by 0 to $N - 1$ cycles before being read out. This introduces a total synchronization overhead of

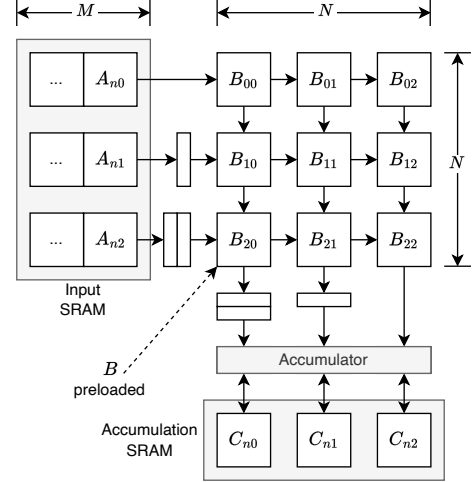


Figure 2. Computing $C += AB$ on a weight-stationary systolic array.

$2N - 1$ cycles. The total computation takes $M + 3N - 1$ cycles, resulting in an array utilization of $\frac{M}{M+3N-1}$. When $M \gg N$, this preloading and synchronization overhead is effectively amortized over the duration of the computation.

2.3 Implementing FlashAttention on Systolic Array Based Accelerators

The FlashAttention algorithm [19, 42] is shown in algorithm 1, focusing on the computational steps and omitting memory load/store operations for brevity. Matrix multiplications are highlighted in red, while non-matrix operations such as reductions and element wise computations are shown in blue. The exponential function is implemented as $\exp(x) = 2^{x \log_2 e}$, following the official open-source FlashAttention implementation, since \exp_2 is typically more efficient than \exp on hardware accelerators.

To implement FlashAttention on systolic array based accelerators, the first matrix multiplication result must be moved out to a vector unit or scalar unit for softmax-related operations. Intermediate results must then be sent back into the array for the second matrix multiplication. As discussed in subsection 2.2, these round-trips incur preloading and synchronization overheads. To amortize them, large tile sizes are preferred. However, larger tiles increase the imbalance between matrix and non-matrix FLOPs and raise SRAM demand for intermediate storage. Even with software pipelining to overlap execution, the FLOPs/s imbalance between matrix multiplications and other operations leads to substantial time spent on non-matrix computations [37]. Achieving high performance for FlashAttention on systolic arrays remains challenging.

Algorithm 1: FlashAttention-2 and 3 forward pass

Require: Matrices $Q, K, V \in \mathbb{R}^{LEN \times d}$

- 1 Divide Q into $T_r = \lceil \frac{LEN}{B_r} \rceil$ blocks of size $B_r \times d$ each, and divide K and V into $T_c = \lceil \frac{LEN}{B_c} \rceil$ blocks of size $B_c \times d$ each;
- 2 **for** $1 \leq i \leq T_r$ **do**
- 3 Initialize $old_m, old_l = (-\infty), (0) \in \mathbb{R}^{B_r}$;
- 4 Initialize $old_O = (0) \in \mathbb{R}^{B_r \times d}$;
- 5 **for** $1 \leq j \leq T_c$ **do**
- 6 $S = Q_i K_j^T \in \mathbb{R}^{B_r \times B_c}$;
- 7 $local_m = rowmax(S) \in \mathbb{R}^{B_r}$;
- 8 $new_m = max(local_m, old_m) \in \mathbb{R}^{B_r}$;
- 9 $a = old_m - new_m \in \mathbb{R}^{B_r}$;
- 10 $b = exp(\frac{a}{\sqrt{d}}) = exp2(\frac{\log_2 e}{\sqrt{d}} a) \in \mathbb{R}^{B_r}$;
- 11 $N = S - new_m \in \mathbb{R}^{B_r \times B_c}$;
- 12 $P = exp(\frac{N}{\sqrt{d}}) = exp2(\frac{\log_2 e}{\sqrt{d}} N) \in \mathbb{R}^{B_r \times B_c}$;
- 13 $local_l = rowsum(P) \in \mathbb{R}^{B_r}$;
- 14 $new_l = old_l \times b + local_l \in \mathbb{R}^{B_r}$;
- 15 $local_O = PV_j \in \mathbb{R}^{B_r \times d}$;
- 16 $new_O = diag(b)old_O + local_O \in \mathbb{R}^{B_r \times d}$;
- 17 $old_m = new_m$;
- 18 $old_l = new_l$;
- 19 $old_O = new_O$;
- 20 **end for**
- 21 $O_i = diag(old_l)^{-1} old_O \in \mathbb{R}^{B_r \times d}$;
- 22 **end for**
- 23

2.4 Motivation

Running the complete FlashAttention algorithm within a single systolic array addresses several critical inefficiencies. By eliminating offloading to external vector or scalar units, all computations can leverage the abundant matrix multiplication FLOPs/s inherently available within the systolic array, significantly improving overall hardware utilization. However, achieving full execution of FlashAttention within the array presents considerable challenges:

- **Efficient Non-MAC Operations:** Operations such as exp, rowmax, and rowsum typically rely on external units due to their element-wise or reduction nature. Implementing these efficiently using only MAC-based PEs requires careful algorithmic transformations and architectural extensions.
- **Computation Overlap:** To maximize utilization, non-matrix operations must be tightly overlapped with ongoing matrix computations. The complex data dependencies within FlashAttention demand a finely tuned scheduling strategy to ensure that overlapping computations do not stall each other.

- **Dataflow and SRAM Management:** The intermediate data produced by the first matrix multiplication in FlashAttention must be effectively reused without excessive SRAM accesses or port contention. Achieving this reuse within the constrained internal storage of the systolic array poses a significant design challenge.

Addressing these challenges requires novel architectural enhancements and sophisticated scheduling algorithms, forming the basis for our proposed FSA architecture and SystolicAttention scheduling algorithm detailed in subsequent sections.

3 FSA Overview

The design principle of FSA is to enable the execution of the full FlashAttention algorithm on a single systolic array with minimal hardware overhead, thereby improving the FLOPs/s for the non-matrix multiplication operations and eliminating the need for an external vector unit. To achieve this, we add a row of comparison units at the top of the array to perform the on-the-fly rowmax operation. Additionally, we introduce a *Split* unit in each PE to implement the exp operation. To allow the rowmax, exp, and rowsum operations to overlap with matrix multiplication, we incorporate an upward data path in the systolic array.

In this section, we first provide an overview of the enhanced systolic array microarchitecture, FSA, that we propose to accelerate the FlashAttention algorithm. We then describe how the non-matrix operations in FlashAttention can be executed using FSA. Finally, we demonstrate how to extensively overlap different computations within FSA in a systolic manner using our proposed SystolicAttention scheduling algorithm.

3.1 FSA Design Overview

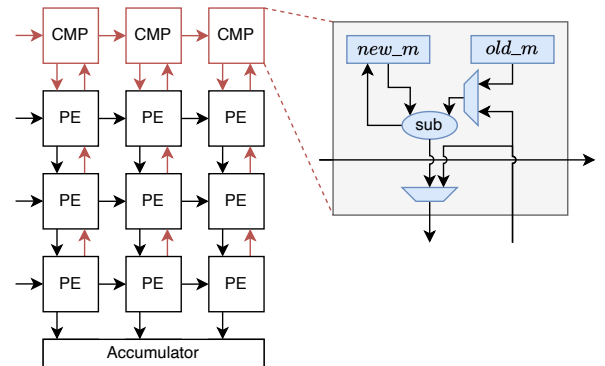


Figure 3. FSA’s modifications to standard systolic array.

As shown in Figure 3, FSA is a systolic array based accelerator that extends the standard architecture with three key modifications to enable efficient execution of FlashAttention:

1. A row of comparison units at the top of the array to compute the column-wise maximum of the output on the fly.
2. A *Split* unit in each PE to decompose the input floating-point value into its integer and fractional parts.
3. An upward data path to propagate partial sums in the reverse direction.

The detailed design of these modifications is as follows:

Row of comparison units: To implement lines 7–9 of [algorithm 1](#), we add a row of comparison units at the top of the array to compute the maximum value of each output column dynamically. Each unit consists of a floating-point adder and two registers. The register *old_m* stores the maximum value from the previous iteration, while *new_m* holds the temporary maximum of the current iteration. The value of *new_m* is updated by comparing *old_m* and the current input using subtraction through the floating-point adder. This differential computation enables efficient max tracking inline with systolic flow.

Split unit in each PE: Each PE is equipped with a *Split* unit that separates the input floating-point number into its integer and fractional components. The exp2 operation is applied to the fractional part using piecewise linear interpolation, which is efficiently handled by the PE’s MAC unit.

Upward data path: Standard systolic arrays propagate partial sums in one direction only. We add an additional data path that enables upward propagation, allowing computation to start from either the top or bottom of the array.

These architectural enhancements allow FSA to support operations that are not feasible on a baseline systolic array, thereby enabling efficient standalone execution of FlashAttention, as elaborated in the following sections.

3.2 rowmax on FSA

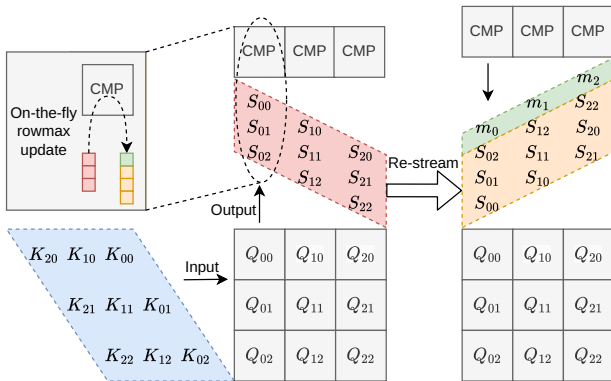


Figure 4. On-the-fly rowmax generation.

[Figure 4](#) illustrates the fused matrix multiplication and rowmax computation, which corresponds to lines 7–9 of [algorithm 1](#). The matrix multiplication $S = Q_i K_j^T$ is performed in the systolic array along the upward data path, such that

the **rows** of S become the **columns** of the systolic array and exit the array from the top.

The rowmax operation is executed in the comparison units concurrently with the generation of each row of S . As the rows of S are produced, they are re-streamed from the top of the array back down through the comparison units. By the time the maximum value of each row is computed, S is already resident in the systolic array.

Consequently, the subtraction operation $N = S - \text{new_m}$ from [line 11](#) of [algorithm 1](#) can be performed immediately. This is achieved by streaming constant ones from the left of the array as the multiplicand, and streaming *new_m* from the top of the array as the addend.

3.3 exp and exp2 on FSA

After the rowmax and subtraction operations, an element-wise exponential function must be applied to the matrix N , as shown in [line 12](#) of [algorithm 1](#):

$$P = \exp\left(\frac{N}{\sqrt{d}}\right) = \exp2\left(\frac{\log_2 e}{\sqrt{d}} \cdot N\right).$$

The exp function is implemented using exp2, which is typically more efficient on hardware accelerators [26]. The constant multiplication $\frac{\log_2 e}{\sqrt{d}} \cdot N$ can be computed by streaming the constant $\frac{\log_2 e}{\sqrt{d}}$ from the left of the array as the multiplicand, since the matrix N is already resident in the systolic array after the subtraction operation. For the element-wise exp2 operation, we use a piecewise linear interpolation to approximate the function [43].

As proposed in [33], the input to exp2 can be split into its integer and fractional parts for a fixed-point number, and the fractional part can be approximated using piecewise linear interpolation. We found that this approach is also applicable to floating-point numbers. The piecewise linear interpolation can be efficiently implemented by reusing the MAC units in the systolic array. A floating-point number x can be decomposed into its integer and fractional components: $x = x_i + x_f$, where x_i is the integer part and x_f is the fractional part [1]. This decomposition leads to the identity:

$$\exp2(x) = 2^{x_i + x_f} = 2^{x_i} \cdot 2^{x_f}.$$

Since $N = S - \text{rowmax}(S)$, all elements in N are less than or equal to zero. This implies $x_f \in (-1, 0]$, and therefore $2^{x_f} \in (0.5, 1]$. Given this limited range for x_f , we find that an 8-piece uniform piecewise linear interpolation is sufficient to achieve a relative error around 10^{-2} in the final FlashAttention results:

$$\exp2(x) \approx 2^{x_i} \cdot (\text{slope}_k \cdot x_f + \text{intercept}_k), \quad k \in [0, 8).$$

As shown in [Figure 5](#), the piecewise linear interpolation for x_f can be implemented by reusing the MAC units in the systolic array. A simple *Split* unit is added to separate the input x into its integer and fractional parts. The *Split* unit extracts x_i and x_f by shifting the mantissa bits to align the

exponent to zero. The term 2^{x_i} affects only the exponent bits in the final result, effectively increasing the exponent by x_i .

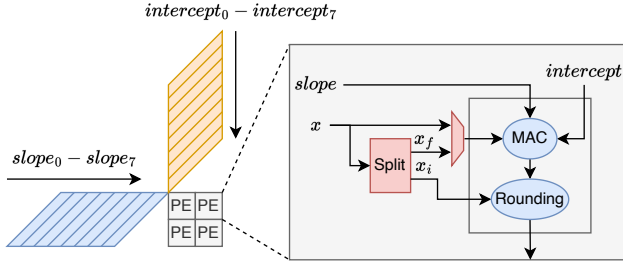


Figure 5. exp2 using piecewise linear interpolation.

To avoid the need for storing the piecewise linear interpolation coefficients in the systolic array, we stream the $slope_k$ and $intercept_k$ values from the left and top of the array, respectively. We further observe that all intercepts lie in the range $(0.5, 1]$, so their exponent can only be 0 or -1 . The MSBs of their exponents can be used to encode the interpolation index k . This enables each PE to update its register based on k without requiring additional control signals.

3.4 rowsum on FSA

Benefiting from the in-place exp computation of $P = \exp\left(\frac{N}{\sqrt{d}}\right)$ in the systolic array, the rowsum operation can begin as soon as the top-left element of P is produced.

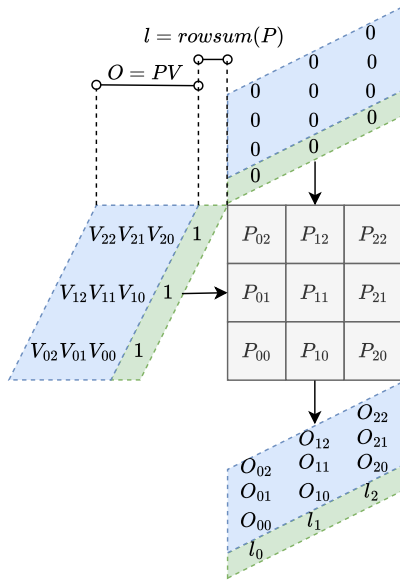


Figure 6. rowsum using systolic array.

As shown in [Figure 6](#), the rowsum of P can be computed by streaming constant ones from the left of the array as the multiplicand, and streaming zeros from the top of the array as the addend. The second matrix multiplication, $O =$

PV can then be performed in the systolic array along the downward data path, starting one cycle after the rowsum operation begins. Once the rowsum $local_l$ and the output $local_O$ exit the array from the bottom, they are accumulated with the previous values old_l and old_O in the accumulator, and the results update new_l and new_O in the accumulation SRAM, respectively.

3.5 Overlapping Computations with SystolicAttention

So far, we have introduced the key operations required to perform FlashAttention within a systolic array, including rowmax, exp2, and rowsum. We now describe how these operations can be overlapped in a systolic fashion to maximize efficiency.

Each iteration of the FlashAttention algorithm involves two matrix multiplications. To avoid costly data movement between the systolic array and external SRAM, we structure computation on an $N_ROWS \times N_COLS$ systolic array by selecting tile sizes $B_r = N_COLS$ and $B_c = N_ROWS = d$. This allows the output of the first matrix multiplication, $S = Q_i K_j^T$, to be directly re-streamed into the array as input for the second matrix multiplication.

During the first matrix multiplication, the head dimension d of both Q and K is mapped to N_ROWS , while the sequence length B_r of Q is mapped to N_COLS . After computing S , we re-stream it from the top of the array, mapping the B_c dimension of S to N_ROWS . A sequence of element-wise operations is then performed in-place cycle by cycle to transform S into N and then into P .

For the second matrix multiplication, $O = PV$, the B_c dimension of V is mapped to N_ROWS and contracted with the stationary matrix P inside the systolic array.

We use the upward data path for the first matrix multiplication, such that the elements of P are generated from the top left to the bottom right of the array. Then, by leveraging the downward data path, we can immediately begin the second matrix multiplication once the top-left element of P is available.

[Figure 7](#) illustrates the execution of the entire inner loop. The fifth operation, $a = old_m - new_m$, passes down the difference between the previous and current maximum values from comparison units to the accumulator. This operation runs in parallel with the constant multiplication $\frac{\log_2 e}{\sqrt{d}} \cdot N$, as the downward data path is idle during the in-place constant multiplication.

Overall, each iteration takes only $2 \times N_COLS + 3 \times N_ROWS + 10$ cycles, meaning that on an $N \times N$ systolic array, it takes just $5N + 10$ cycles to process a $N \times N$ FlashAttention tile. By contrast, on a naive $N \times N$ systolic array, the two independent matrix multiplications alone may require up to $8N - 2$ cycles due to preloading and synchronization overheads discussed in [subsection 2.2](#).

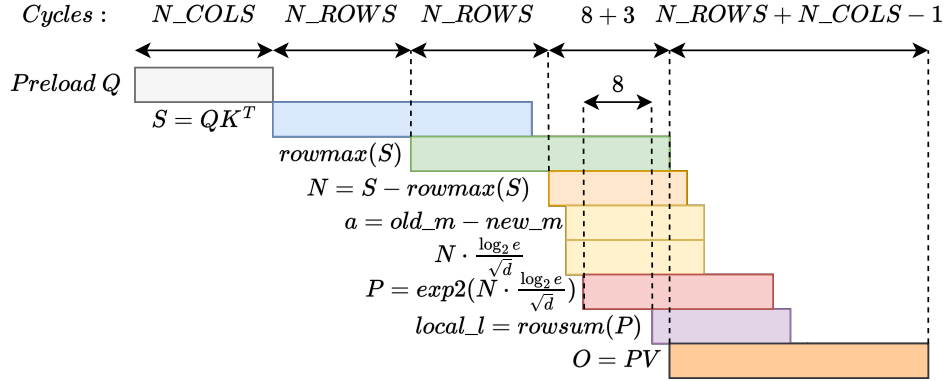


Figure 7. Overlapped computations of the FlashAttention inner loop in the systolic array.

The re-scaling operation in line 21 of algorithm 1 is only performed once per outer loop. It is executed using the accumulator after the second matrix multiplication completes. In our implementation, this re-scaling step takes $2N + 20$ cycles, which is negligible compared to the inner loop execution time.

4 FSA Microarchitecture

FSA modifies the standard systolic array architecture to support the SystolicAttention algorithm. To validate its feasibility and quantify the associated hardware overhead, we implement FSA in RTL and design a minimal yet flexible instruction set capable of executing the full FlashAttention.

The RTL design is implemented in Chisel HDL [12] and built using the Chipyard [4–6, 18] framework for system-on-chip (SoC) construction. Unlike prior efforts such as Gemini [21], which focus on flexible design space exploration, our goal is to deliver a concrete and complete implementation of FSA to validate both the practicality of the SystolicAttention algorithm and its hardware cost.

This section provides an overview of the FSA microarchitecture, details the instruction set design that simplifies the hardware implementation, and describes the systolic array controller that orchestrates the execution of the SystolicAttention algorithm.

4.1 Microarchitecture Overview

An overview of the FSA microarchitecture is shown in Figure 8. FSA receives instructions via an AXI4-Lite interface and accesses backing memory through a configurable number of AXI4 memory interfaces.

The instruction decoder classifies instructions into three types: *load*, *store*, and *compute*. Instructions of different classes are executed asynchronously, while instructions of the same class are issued in order but their execution may be interleaved.

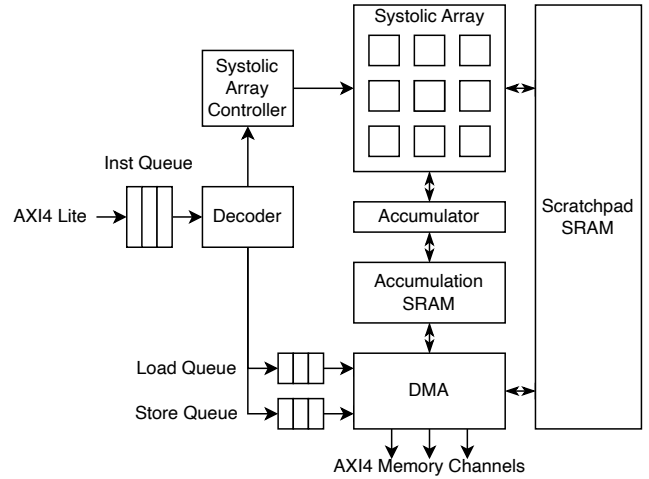


Figure 8. FSA microarchitecture.

The systolic array controller issues compute instructions once the required data has been loaded into SRAM. To simplify control logic, FSA prioritizes SRAM access over compute operations, making the latency of compute instructions fully deterministic once issued. This design allows the controller to statically schedule control signals based on the known execution cycle of each instruction.

The DMA engine follows an iDMA-style interface [13] and supports 2D data transfers. Each DMA instruction can specify source and destination addresses in SRAM and backing memory, along with the transfer size and stride.

When multiple AXI4 channels are available, the DMA engine automatically partitions the transfer into parallel AXI4 transactions, maximizing memory bandwidth utilization.

4.2 FSA Instruction Set

To enable fine-grained overlap between various FlashAttention operations, the systolic array in FSA requires more sophisticated control logic than standard systolic arrays. The primary design goal of the FSA instruction set is to ensure

that compute instructions execute in a fully deterministic manner, independent of memory access latency. This simplification greatly reduces control complexity.

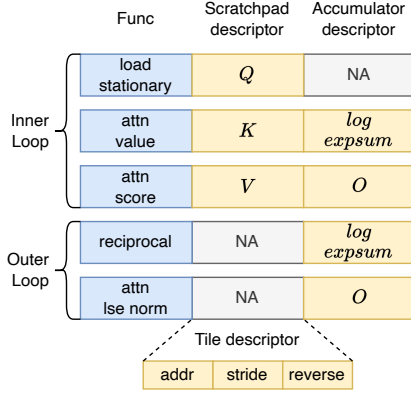


Figure 9. FSA compute instructions.

To achieve this, we define five compute instructions based on their SRAM data dependencies, as illustrated in Figure 9. The FlashAttention inner loop is divided into three phases:

- **Load Stationary:** Preload Q into the systolic array.
- **Attn Score:** Perform the first matrix multiplication using Q and K , fused with element-wise online softmax to compute the P matrix in-place within the systolic array. The log of the exponent sum for P is also calculated during this step.
- **Attn Value:** Perform the second matrix multiplication using V and P .

The FlashAttention outer loop is divided into two additional phases:

- **Reciprocal:** Load the log exponent sum of P from the accumulation SRAM and compute its reciprocal. The result is stored in the accumulator as a scaling factor for the next phase.
- **Attn LSE Norm:** Load the output matrix O from the accumulator and apply the reciprocal scaling factor.

Each compute instruction reads one input tile from SRAM and writes one output tile to the accumulator SRAM. This one-tile-in, one-tile-out design ensures that compute instructions can be executed as soon as their corresponding SRAM tile is ready—without waiting on other tiles to be loaded or processed.

DMA instructions follow a similar structure to compute instructions, consisting of one memory tile descriptor and one SRAM tile descriptor. However, they use wider bit fields to support large memory address spaces.

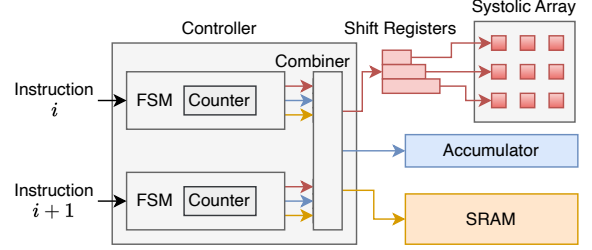


Figure 10. FSA systolic array controller.

4.3 Systolic Array Controller

The microarchitecture of the FSA systolic array controller is illustrated in Figure 10. The controller comprises two identical counter-based finite state machines (FSMs), each responsible for generating control signals for a compute instruction.

Control signals are categorized into three types:

- **PE Control Signals:** Define the operations to be performed within the PEs of the systolic array.
- **Accumulator Control Signals:** Specify the actions performed in the accumulator.
- **SRAM Control Signals:** Govern the read and write operations to SRAM required for executing the compute instruction.

Because compute instruction execution is fully deterministic, the counter is initialized at the start of each compute instruction, incremented every cycle, and reset to zero upon completion. As a result, the FSMs can generate control signals solely based on the instruction type and the current counter value.

To simplify control logic development, we implemented a domain specific language (DSL) on top of Chisel and Scala. This DSL allows designers to specify which control signals should be scheduled at each cycle. The control logic is then automatically synthesized from the DSL specification.

The dual-FSM architecture enables overlapping execution of two compute instructions. For example, the *Attn Value* instruction can begin as soon as the *Attn Score* instruction produces the first element of the P matrix. A combiner unit merges the control signals from both FSMs, ensuring that signals are emitted in the correct order and that conflicts are avoided.

5 FSA Kernel Programming Model

The AWS Neuron Kernel Interface (NKI) [11] provides an expressive Python interface that allows users to write custom kernels for AWS Neuron devices. It offers instruction-level control with the convenience of Python APIs.

Inspired by AWS NKI, FSA provides a similar, simplified Python library for writing custom FSA kernels. The library consists of three main components: type-safe tensors, a Python API for the FSA instruction set, and a lightweight JIT compiler.

5.1 Type-Safe Tensors

The FSA Python library implements a PyTorch-like [7, 39] tensor abstraction for representing multi-dimensional arrays. Because the memory hierarchy is fully user-managed, tensors can be allocated in one of three memory spaces: main memory, scratchpad SRAM, or accumulation SRAM. Accordingly, we define three tensor types:

- MTile — for main memory tensors,
- STile — for scratchpad SRAM tensors,
- ATile — for accumulation SRAM tensors.

All tensor types support a subset of the PyTorch API, including shape, dtype, split, and reverse. By explicitly distinguishing tensor types, users can write custom kernel functions that clearly declare the expected input and output tensor memory scopes.

5.2 Python API for FSA Instructions

Each FSA instruction is exposed through a corresponding Python API. These APIs are designed to be type-safe, ensuring correct usage of tensor types. The complete set of supported APIs is shown in Listing 1.

Listing 1. FSA Python instructions.

```
# DMA Instructions
def store_tile(src: ATile, dst: MTile, ...)
def load_tile(src: MTile, dst: STile, ...)
# Compute Instructions
def load_stationary(tile: STile, ...)
def attn_score(K: STile, l: ATile, ...)
def attn_value(V: STile, O: ATile, ...)
def reciprocal(l: ATile, ...)
def attn_lse_norm(O: ATile, ...)
```

Internally, these functions construct hardware instructions using the metadata of the input tensors—such as shape, stride, and data type. This abstraction allows users to write high-level kernels without managing low-level hardware details.

5.3 JIT Kernel Compiler

We provide a lightweight JIT compiler that compiles decorated Python functions into FSA binary programs. These programs consist of a sequence of binary instructions that can be submitted to the device’s instruction queue for execution.

The FlashAttention kernel implemented in FSA using the JIT compiler is shown in Listing 2.

Listing 2. FSA FlashAttention kernel.

```
import fsa as F

@F.kernel(device="verilator_sim")
def attention(Q: MTile, K: MTile, Vt: MTile)
    -> MTile:
    # allocate output tensor
```

```
Ot: MTile = F.alloc_mem(..)
# split large tensors into tiles
Ot_MTiles = Ot.split(br, dim=-1) # [d, br]
Q_MTiles = Q.split(br, dim=-2) # [br, d]
K_MTiles = K.split(bc, dim=-2) # [br, d]
Vt_MTiles = Vt.split(bc, dim=-1) # [d, bc]
# double buffering for Q, K, Vt
K_STiles = (F.alloc_spad(..), F.alloc_spad(..))
Vt_STiles = (F.alloc_spad(..), F.alloc_spad(..))
# allocate space for accumulation results
log_expsum = F.alloc_accum(..) # [1, br]
Ot_ATile = F.alloc_accum(..) # [d, br]

for i, Q_i in enumerate(Q_MTiles):
    F.load_tile(Q_i, Q_STiles[i % 2])
    for j, (K_j, Vt_j) in enumerate(zip(K_MTiles, Vt_MTiles)):
        F.load_stationary(Q_STiles[i % 2])
        F.load_tile(K_j, K_STiles[j % 2])
        F.attn_score(K_STiles[j % 2], log_expsum)
        F.load_tile(Vt_j, Vt_STiles[j % 2])
        F.attn_value(Vt_STiles[j % 2], Ot_ATile)
    F.reciprocal(log_expsum)
    F.attn_lse_norm(Ot_ATile)
    F.store_tile(Ot_ATile, Ot_MTiles[i])

# Run simulation and return result
Ot = attention(Q, K, Vt)
O = Ot.to_numpy().T # Host-side transpose
```

The JIT compiler processes Python functions decorated with `@F.kernel`. The decorator also specifies the target device (e.g., a Verilator-based simulator [48]), and handles device-host communication automatically.

In the example above, the host loads input tensors into device memory using DRAMSim2 [41], dispatches the compiled instructions to the FSA device, and retrieves the output tensors upon completion. Because FSA does not currently support hardware matrix transposition, the input matrix V is transposed in advance, and the output matrix O is converted to NumPy [25] arrays for post-processing. On commercial hardware, such transpositions can be performed by the DMA engine during memory transfers [11], and therefore should not incur significant overhead.

6 Evaluation

6.1 FlashAttention Performance

We compare the FlashAttention performance of FSA with state-of-the-art commercial systolic-array-based accelerators, including Google’s TPUv5e [24] and AWS NeuronCore-v2 [9]. We select TPUv5e because it has the same systolic array size, 128×128 , as AWS NeuronCore-v2. For fairness,

we also configure FSA with a 128×128 systolic array. All accelerators use 16-bit floating point activation and 32-bit accumulation.

The accelerator configurations used for evaluation are summarized in Table 1. We evaluate the FlashAttention forward pass performance of a single attention head on all three accelerators, using a head dimension of 128, without causal masking, and with sequence lengths ranging from 2048 to 16384.

To clarify, we use the term *FLOPs* to denote the number of floating-point operations, and *FLOPs/s* to indicate the number of floating-point operations performed per second. Although all accelerators share the same systolic array size, their absolute performance still varies due to differences in clock frequency, which in turn depend on the specific node technology employed. Therefore, we simulate FSA at 1.5 GHz, a target that is achievable in 16 nm technology, as discussed in subsection 6.3, and compare matrix multiplication FLOPs/s utilization rather than wall-clock execution time. This metric reflects the end-to-end absolute performance of each accelerator under the same clock frequency.

Table 1. Accelerator configurations used for evaluation.

Accelerator	TPUv5e	Neuron-v2	FSA
Systolic array size	128	128	128
Number of arrays	4	1	1
TFLOPs/s (MAC only)	196.6	91.75	32.77
Frequency	1.5GHz ¹	2.8GHz	1.5GHz
Memory Bandwidth	819GB/s	820GB/s	820GB/s
Scratchpad SRAM	48MiB	24MiB	192KiB ²
Accumulation SRAM		2MiB	64KiB
Require Vector Unit?	Yes	Yes	No

¹ The clock frequency of TPUv5e is inferred from its reported performance using the formula: $\text{freq}_{\text{GHz}} = \frac{\text{TFLOPs} \cdot 10^{12}}{2 \cdot 128 \cdot 128 \cdot 10^9}$.

² Since FSA operates on 128×128 tiles and only targets FlashAttention operations in this experiment, 192 KiB of SRAM is sufficient to support the algorithm using double buffering.

The number of floating-point operations in FlashAttention [19] is given by:

$$\text{Total FLOPs} = 4 \times \text{SeqLen}^2 \times d$$

where SeqLen is the sequence length and d is the head dimension.

We calculate the achieved FLOPs/s on each accelerator as follows:

$$\text{Achieved FLOPs/s} = \frac{\text{Total FLOPs}}{\text{Execution Time}}$$

and the FLOPs/s utilization as:

$$\text{FLOPs/s Utilization} = \frac{\text{Achieved FLOPs/s}}{\text{Peak FLOPs/s}}$$

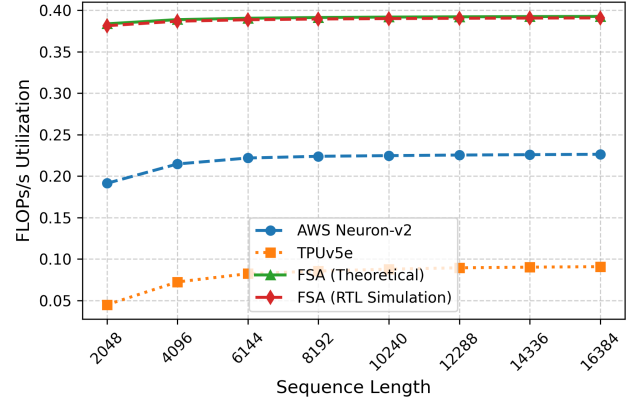


Figure 11. FlashAttention FLOPs/s utilization of FSA compared to TPUv5e and AWS NeuronCore-v2.

We use the official FlashAttention kernel implementations for the two commercial accelerators, which are optimized for their respective architectures:

- `jax.experimental.pallas.ops.tpu.flash_attention` for the TPUv5e [27].
- `neuronxcc.nki.kernels.attention.flash_fwd` for the AWS NeuronCore-v2 [11].

The experimental results are shown in Figure 11. Benefiting from intensively overlapped computations, FSA achieves average FLOPs/s utilization that is 1.77 times and 4.83 times higher compared to TPUv5e and AWS NeuronCore-v2, respectively. Moreover, the results confirm that our RTL implementation of FSA closely aligns with the theoretical performance outlined in subsection 3.5, validating the correctness of our RTL design.

6.2 Accuracy Analysis

The SystolicAttention produces mathematically equivalent results to standard attention and preserves the order of floating-point operations. However, due to the piecewise linear interpolation used for the \exp_2 computation, the final results may differ slightly from those generated by commercial accelerators.

In this section, we first analyze the accuracy of the piecewise linear approximation of the single \exp_2 function. We then assess its overall impact on the final attention results.

6.2.1 Error Analysis of Piecewise Linear Approximation

Since the input to the \exp_2 function in the FlashAttention is always negative, we exhaustively evaluate the piecewise linear approximation over all negative normal fp16 values. We exclude subnormal values, as they are typically flushed to zero in most accelerators [22].

Figure 12 shows the mean absolute error (MAE) and mean relative error (MRE) of the piecewise linear approximation of the \exp_2 function, plotted against the number of segments

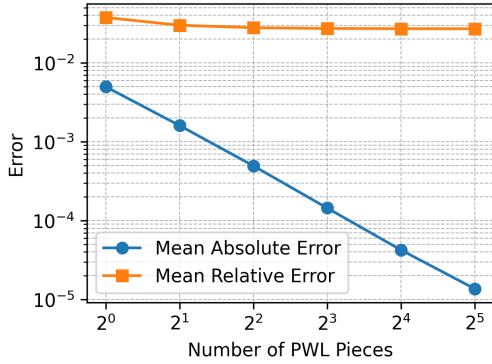


Figure 12. exp2 piecewise linear interpolation error analysis.

used in the approximation. The MAE decreases significantly as the number of segments increases, while the MRE remains relatively stable. This occurs because the breakpoints in the approximation are uniformly spaced, whereas the fp16 representation is logarithmic in nature, making relative error more sensitive for values close to zero. We choose to use 8 segments in our FSA implementation, which achieves a MAE of 0.00014 and an MRE of 0.02728. Although non-uniformly spaced breakpoints could further reduce the MRE, we leave this exploration for future work.

6.2.2 Overall FlashAttention Accuracy. To evaluate the accuracy of the FlashAttention attention on FSA, we compare it against `torch.nn.functional.scaled_dot_product_attention` in PyTorch [7]. We use the same head dimension and sequence lengths as in the performance evaluation. The input matrices are randomly generated using the same distribution as in the FlashAttention-3 [42] accuracy evaluation:

$$Q, K, V \sim \mathcal{N}(0, 1) + \mathcal{N}(0, 100) \cdot \text{Bernoulli}(0.001).$$

Table 2. Mean absolute error (MAE), root mean squared error (RMSE), and mean relative error (MRE) of the FlashAttention results on FSA.

SeqLen	MAE	RMSE	MRE
2048	7.983e-03	1.315e-02	1.558e-02
4096	1.379e-02	2.290e-02	2.596e-02
6144	1.849e-02	3.085e-02	3.545e-02
8192	2.253e-02	3.772e-02	4.413e-02
10240	2.595e-02	4.373e-02	5.259e-02
12288	2.890e-02	4.873e-02	5.920e-02
14336	3.165e-02	5.351e-02	6.529e-02
16384	3.403e-02	5.784e-02	7.181e-02

The overall accuracy results are summarized in Table 2. The MAE lies in the range of 7×10^{-3} to 4×10^{-2} , while the MRE ranges from 1×10^{-2} to 8×10^{-2} . These results indicate that the piecewise linear approximation of the exp2 function has a negligible impact on the final attention output.

6.3 FSA Area Overhead

The area overhead of FSA arises from the following additional components:

- The upward data path, in addition to the standard downward path, enabling partial sums to propagate in both directions.
- A top row of *CMP* units, responsible for identifying the maximum value in each systolic array column.
- A *Split* unit within each PE, which separates input values into integer and fractional parts for the exp2 operation.

To evaluate the area overhead, we synthesize the systolic array portion of FSA, excluding SRAMs and DMA, at 1.5 GHz using a 16 nm commercial process. The resulting area breakdown is shown in Table 3.

Table 3. FSA area breakdown.

Group	Component	Area (%)	Area (μm^2)
Standard	PEs	86.81	24445044
	Other logic	1.11	313457
	<i>Total</i>	87.92	24758501
FSA additional	Upward data path	6.24	1756641
	Split units	5.30	1493150
	CMP units	0.53	149524
	<i>Total</i>	12.07	2029891

As shown in Table 3, the standard systolic array occupies 87.92% of the total area, while FSA’s additional components contribute 12.07%. The dominant sources of overhead are the upward data path and the *Split* units, which account for 6.24% and 5.30% of the total area, respectively. This is due to their replication across all PEs in the 128×128 array. In contrast, the *CMP* units contribute only 0.53%, as they are instantiated solely in the top row of the array.

7 Related Work

Significant efforts have been made to fuse FlashAttention on hardware accelerators. COSA [47] and COSA Plus [46] fuse FlashAttention across two cooperative systolic arrays, but data from the first array must still pass through a special function unit (SFU) for softmax. Matching SFU throughput to large systolic arrays can increase hardware cost. FuseMax [37] builds on the cascade Einsum abstraction introduced in TeAAL [36] to describe the FlashAttention algorithm and map it onto spatial accelerator models. FuseMax

uses a different dataflow from the one used in our paper: by employing an output-stationary dataflow, it overlaps four FlashAttention iterations on the systolic array to obtain very high utilization. The overlapping of iterations necessitates storing multiple input tiles in SRAM and maintaining intermediate results within the array, leading to higher storage overhead and control complexity. Additionally, FuseMax assumes all FlashAttention operations are performed in fp16 format. In contrast, the original FlashAttention algorithm uses fp16 for matrix multiplications but fp32 for accumulations. Reconciling this difference may require intermediate results to be stored in fp32, which can further increase register usage. ExpMul [3] fuses the exp and the second matrix multiplication in FlashAttention, which is orthogonal to our work and could be integrated into FSA as well.

8 Discussion

8.1 Necessity of a Vector Unit

While FSA is capable of executing FlashAttention entirely on the systolic array without relying on a vector unit, a vector unit or SFU is still necessary in a full accelerator system to support activation functions outside of FlashAttention. However, because FSA offloads all attention-related computation from the vector unit, the overall vector FLOPs/s requirement may be significantly reduced.

8.2 FSA Variant: Area-Optimized Design

This paper focuses on the most performant FSA variant, which uses both upward and downward data flow to maximize throughput.

However, during development, we also explored a simpler variant with a single data flow direction, similar to a standard systolic array. This configuration still supports the SystolicAttention algorithm, but introduces additional latency: the second matrix multiplication ($O = PV$) cannot begin immediately after the first elements of P are computed and must wait for the entire P matrix.

This results in the inner loop latency increasing from $5N + 10$ to $6N + 10$ cycles. Despite this, this area-optimized design would still deliver higher FLOPs/s utilization than commercial accelerators.

8.3 Limitations of FSA

Although FSA delivers high FLOPs/s utilization for FlashAttention, it is not well-suited for the decoding phase of LLM inference.

FSA is ideal for the (1) LLM training and (2) prefill phase of LLM inference, where the query matrix Q has a long sequence length, making the attention computation compute-intensive [40]. In this case, the high FLOPs/s throughput of FSA effectively accelerates the workload.

In contrast, during the decoding phase, the query Q has a sequence length of 1, making the computation memory-bound. Moreover, since FSA operates on 128×128 tiles, Q must be padded to fit this shape, resulting in substantial wasted computation and inefficient resource usage.

9 Conclusion

We have presented FSA, an enhanced systolic array architecture that enables complete FlashAttention computation within a single systolic array. At the core of our approach is the SystolicAttention algorithm, which achieves extensive element-wise overlap of all FlashAttention operations through careful scheduling and static data flow management.

The experimental results validate our approach, showing significant improvements in FLOPs/s utilization compared to state-of-the-art commercial accelerators while maintaining high accuracy and requiring minimal on-chip memory.

References

- [1] 2019. IEEE Standard for Floating-Point Arithmetic. *IEEE Std 754-2019 (Revision of IEEE 754-2008)* (2019), 1–84. doi:10.1109/IEEESTD.2019.8766229
- [2] Ahmed J. Abdelmaksoud, Shady Agwa, and Themis Prodromakis. 2024. DiP: A Scalable, Energy-Efficient Systolic Array for Matrix Multiplication Acceleration. arXiv:2412.09709 [cs.AR] <https://arxiv.org/abs/2412.09709>
- [3] Kosmas Alexandridis, Vasileios Titopoulos, and Giorgos Dimi-trakopoulos. 2025. Low-Cost FlashAttention with Fused Exponential and Multiplication Hardware Operators. arXiv:2505.14314 [cs.AR] <https://arxiv.org/abs/2505.14314>
- [4] Alon Amid, David Biancolin, Abraham Gonzalez, Daniel Grubb, Sagar Karandikar, Harrison Liew, Albert Magyar, Howard Mao, Albert Ou, Nathan Pemberton, Paul Rigge, Colin Schmidt, John Wright, Jerry Zhao, Jonathan Bachrach, Sophia Shao, Borivoje Nikolić, and Krste Asanović. 2020. Invited: Chipyard - An Integrated SoC Research and Implementation Environment. In *2020 57th ACM/IEEE Design Automation Conference (DAC)*. 1–6. doi:10.1109/DAC18072.2020.9218756
- [5] Alon Amid, David Biancolin, Abraham Gonzalez, Daniel Grubb, Sagar Karandikar, Harrison Liew, Albert Magyar, Howard Mao, Albert Ou, Nathan Pemberton, Paul Rigge, Colin Schmidt, John Wright, Jerry Zhao, Yakun Sophia Shao, Krste Asanović, and Borivoje Nikolić. 2020. Chipyard: Integrated Design, Simulation, and Implementation Framework for Custom SoCs. *IEEE Micro* 40, 4 (2020), 10–21. doi:10.1109/MM.2020.2996616
- [6] Alon Amid, Albert Ou, Krste Asanović, Yakun Sophia Shao, and Borivoje Nikolić. 2021. Vertically Integrated Computing Labs Using Open-Source Hardware Generators and Cloud-Hosted FPGAs. In *2021 IEEE International Symposium on Circuits and Systems (ISCAS)*. 1–5. doi:10.1109/ISCAS51556.2021.9401515
- [7] Jason Ansel, Edward Yang, Horace He, Natalia Gimelshein, Animesh Jain, Michael Voznesensky, Bin Bao, Peter Bell, David Berard, Evgeni Burovski, Geeta Chauhan, Anjali Chourdia, Will Constable, Alban Desmaison, Zachary DeVito, Elias Ellison, Will Feng, Jiong Gong, Michael Gschwind, Brian Hirsh, Sherlock Huang, Kshiteej Kalam-barkar, Laurent Kirsch, Michael Lazos, Mario Lezcano, Yanbo Liang, Jason Liang, Yinghai Lu, C. K. Luk, Bert Maher, Yunjie Pan, Christian Puhersch, Matthias Reso, Mark Saroufim, Marcos Yukio Siraichi, Helen Suk, Shunting Zhang, Michael Suo, Phil Tillet, Xu Zhao, Eikan Wang, Keren Zhou, Richard Zou, Xiaodong Wang, Ajit Mathews, William

- Wen, Gregory Chanan, Peng Wu, and Soumith Chintala. 2024. PyTorch 2: Faster Machine Learning Through Dynamic Python Bytecode Transformation and Graph Compilation. In *Proceedings of the 29th ACM International Conference on Architectural Support for Programming Languages and Operating Systems, Volume 2* (La Jolla, CA, USA) (ASPLOS '24). Association for Computing Machinery, New York, NY, USA, 929–947. doi:10.1145/3620665.3640366
- [8] Bahar Asgari, Ramyad Hadidi, and Hyesoon Kim. 2020. MEISSA: Multiplying Matrices Efficiently in a Scalable Systolic Architecture. In *2020 IEEE 38th International Conference on Computer Design (ICCD)*. 130–137. doi:10.1109/ICCD50377.2020.00036
- [9] AWS Neuron Documentation. 2024. *NeuronCore-v2 Architecture*. <https://awsdocs-neuron.readthedocs-hosted.com/en/latest/general/arch/neuron-hardware/neuron-core-v2.html#neuroncores-v2-arch> Accessed: 2025-06-15.
- [10] AWS Neuron Documentation. 2024. *Trainium/Inferentia2 Architecture Guide for NKI*. https://awsdocs-neuron.readthedocs-hosted.com/en/latest/general/nki/arch/trainium_inferentia2_arch.html#trainium-inferentia2-arch Accessed: 2025-06-15.
- [11] AWS Neuron Team. 2025. AWS Neuron NKI Samples. <https://github.com/aws-neuron/nki-samples>. Accessed: 2025-06-30.
- [12] Jonathan Bachrach, Huy Vo, Brian Richards, Yunsup Lee, Andrew Waterman, Rimas Avizienis, John Wawrzyniek, and Krste Asanović. 2012. Chisel: constructing hardware in a Scala embedded language. In *Proceedings of the 49th Annual Design Automation Conference* (San Francisco, California) (DAC '12). Association for Computing Machinery, New York, NY, USA, 1216–1225. doi:10.1145/2228360.2228584
- [13] Thomas Benz, Michael Rogenmoser, Paul Scheffler, Samuel Riedel, Alessandro Ottaviano, Andreas Kurth, Torsten Hoefler, and Luca Benini. 2024-01. A High-performance, Energy-efficient Modular DMA Engine Architecture. *IEEE Trans. Comput.* 73, 1 (2024-01), 263 – 277. doi:10.3929/ethz-b-000641982
- [14] Tom B. Brown, Benjamin Mann, Nick Ryder, Melanie Subbiah, Jared Kaplan, Prafulla Dhariwal, Arvind Neelakantan, Pranav Shyam, Girish Sastry, Amanda Askell, Sandhini Agarwal, Ariel Herbert-Voss, Gretchen Krueger, Tom Henighan, Rewon Child, Aditya Ramesh, Daniel M. Ziegler, Jeffrey Wu, Clemens Winter, Christopher Hesse, Mark Chen, Eric Sigler, Mateusz Litwin, Scott Gray, Benjamin Chess, Jack Clark, Christopher Berner, Sam McCandlish, Alec Radford, Ilya Sutskever, and Dario Amodei. 2020. Language models are few-shot learners. In *Proceedings of the 34th International Conference on Neural Information Processing Systems* (Vancouver, BC, Canada) (NIPS '20). Curran Associates Inc., Red Hook, NY, USA, Article 159, 25 pages.
- [15] Nicolas Carion, Francisco Massa, Gabriel Synnaeve, Nicolas Usunier, Alexander Kirillov, and Sergey Zagoruyko. 2020. End-to-End Object Detection with Transformers. In *Computer Vision – ECCV 2020: 16th European Conference, Glasgow, UK, August 23–28, 2020, Proceedings, Part I* (Glasgow, United Kingdom). Springer-Verlag, Berlin, Heidelberg, 213–229. doi:10.1007/978-3-030-58452-8_13
- [16] Yu-Hsin Chen, Joel Emer, and Vivienne Sze. 2016. Eyeriss: A Spatial Architecture for Energy-Efficient Dataflow for Convolutional Neural Networks. In *2016 ACM/IEEE 43rd Annual International Symposium on Computer Architecture (ISCA)*. 367–379. doi:10.1109/ISCA.2016.40
- [17] Yu-Hsin Chen, Tushar Krishna, Joel S. Emer, and Vivienne Sze. 2017. Eyeriss: An Energy-Efficient Reconfigurable Accelerator for Deep Convolutional Neural Networks. *IEEE Journal of Solid-State Circuits* 52, 1 (2017), 127–138. doi:10.1109/JSSC.2016.2616357
- [18] Henry Cook, Wesley Terpstra, and Yunsup Lee. 2017. Diplomatic Design Patterns: A TileLink Case Study. In *Proceedings of the First Workshop on Computer Architecture Research with RISC-V (CARRV'17)*. Boston, MA, USA, 1–7.
- [19] Tri Dao. 2023. FlashAttention-2: Faster Attention with Better Parallelism and Work Partitioning. arXiv:2307.08691 [cs.LG] <https://arxiv.org/abs/2307.08691>
- [20] Jacob Devlin, Ming-Wei Chang, Kenton Lee, and Kristina Toutanova. 2019. BERT: Pre-training of Deep Bidirectional Transformers for Language Understanding. In *North American Chapter of the Association for Computational Linguistics*. <https://api.semanticscholar.org/CorpusID:52967399>
- [21] Hasan Genc, Seah Kim, Alon Amid, Ameer Haj-Ali, Vignesh Iyer, Pranav Prakash, Jerry Zhao, Daniel Grubb, Harrison Liew, Howard Mao, Albert Ou, Colin Schmidt, Samuel Steffl, John Wright, Ion Stoica, Jonathan Ragan-Kelley, Krste Asanovic, Borivoje Nikolic, and Yakun Sophia Shao. 2022. *Gemmini: Enabling Systematic Deep-Learning Architecture Evaluation via Full-Stack Integration*. IEEE Press, 769–774. <https://doi.org/10.1109/DAC18074.2021.9586216>
- [22] Google Cloud. 2019. bfloat16: The secret to high performance on Cloud TPUs. <https://cloud.google.com/blog/products/ai-machine-learning/bfloat16-the-secret-to-high-performance-on-cloud-tpus>. Accessed: 2025-06-27.
- [23] Google Cloud. 2024. *TPU Architecture*. <https://cloud.google.com/tpu/docs/system-architecture-tpu-vm> Accessed: 2025-06-15.
- [24] Google Cloud. 2025. *Cloud TPU v5e Documentation*. <https://cloud.google.com/tpu/docs/v5e> Accessed: 2025-06-15.
- [25] Charles R Harris, K Jarrod Millman, Stéfan J van der Walt, Ralf Gommers, Pauli Virtanen, David Cournapeau, Eric Wieser, Julian Taylor, Sebastian Berg, Nathaniel J Smith, et al. 2020. Array programming with NumPy. *Nature* 585, 7825 (2020), 357–362. doi:10.1038/s41586-020-2649-2
- [26] Muhammad Awais Hussain, Shung-Wei Lin, and Tsung-Han Tsai. 2022. An Area-Efficient and High Throughput Hardware Implementation of Exponent Function. In *2022 IEEE International Symposium on Circuits and Systems (ISCAS)*. 3369–3372. doi:10.1109/ISCAS48785.2022.9937238
- [27] JAX Developers. [n. d.]. JAX Pallas TPU Documentation. <https://docs.jax.dev/en/latest/pallas/tpu/index.html>. Accessed: 2025-06-30.
- [28] Norm Jouppi, George Kurian, Sheng Li, Peter Ma, Rahul Nagarajan, Lifeng Nai, Nishant Patil, Suvinay Subramanian, Andy Swing, Brian Towles, Clifford Young, Xiang Zhou, Zongwei Zhou, and David A Patterson. 2023. TPU v4: An Optically Reconfigurable Supercomputer for Machine Learning with Hardware Support for Embeddings. In *Proceedings of the 50th Annual International Symposium on Computer Architecture* (Orlando, FL, USA) (ISCA '23). Association for Computing Machinery, New York, NY, USA, Article 82, 14 pages. doi:10.1145/3579371.3589350
- [29] Norman P. Jouppi, Cliff Young, Nishant Patil, David Patterson, Gaurav Agrawal, Raminder Bajwa, Sarah Bates, Suresh Bhatia, Nan Boden, Al Borchers, Rick Boyle, Pierre-luc Cantin, Clifford Chao, Chris Clark, Jeremy Coriell, Mike Daley, Matt Dau, Jeffrey Dean, Ben Gelb, Tara Vazir Ghaemmaghami, Rajendra Gottipati, William Gulland, Robert Hagmann, C. Richard Ho, Doug Hogberg, John Hu, Robert Hundt, Dan Hurt, Julian Ibarz, Aaron Jaffey, Alek Jaworski, Alexander Kaplan, Harshit Khaitan, Daniel Killebrew, Andy Koch, Naveen Kumar, Steve Lacy, James Laudon, James Law, Diemthu Le, Chris Leary, Zhuyuan Liu, Kyle Lucke, Alan Lundin, Gordon MacKean, Adriana Maggiore, Maire Mahony, Kieran Miller, Rahul Nagarajan, Ravi Narayanaswami, Ray Ni, Kathy Nix, Thomas Norrie, Mark Omernick, Narayana Penukonda, Andy Phelps, Jonathan Ross, Matt Ross, Amir Salek, Emad Samadiani, Chris Severn, Gregory Sizikov, Matthew Snelham, Jed Souter, Dan Steinberg, Andy Swing, Mercedes Tan, Gregory Thorson, Bo Tian, Horia Toma, Erick Tuttle, Vijay Vasudevan, Richard Walter, Walter Wang, Eric Wilcox, and Doe Hyun Yoon. 2017. In-Datacenter Performance Analysis of a Tensor Processing Unit. *SIGARCH Comput. Archit. News* 45, 2 (June 2017), 1–12. doi:10.1145/3140659.3080246
- [30] Sheng-Chun Kao, Suvinay Subramanian, Gaurav Agrawal, Amir Yazdanbakhsh, and Tushar Krishna. 2023. FLAT: An Optimized Dataflow for Mitigating Attention Bottlenecks. In *Proceedings of the 28th ACM*

- International Conference on Architectural Support for Programming Languages and Operating Systems, Volume 2* (Vancouver, BC, Canada) (ASPLOS 2023). Association for Computing Machinery, New York, NY, USA, 295–310. doi:10.1145/3575693.3575747
- [31] Jared Kaplan, Sam McCandlish, Tom Henighan, Tom B. Brown, Benjamin Chess, Rewon Child, Scott Gray, Alec Radford, Jeffrey Wu, and Dario Amodei. 2020. Scaling Laws for Neural Language Models. arXiv:2001.08361 [cs.LG] <https://arxiv.org/abs/2001.08361>
- [32] Hansung Kim, Ruohan Richard Yan, Joshua You, Tieliang Vamber Yang, and Yakun Sophia Shao. 2025. Virgo: Cluster-level Matrix Unit Integration in GPUs for Scalability and Energy Efficiency. In *Proceedings of the 30th ACM International Conference on Architectural Support for Programming Languages and Operating Systems, Volume 2* (Rotterdam, Netherlands) (ASPLOS '25). Association for Computing Machinery, New York, NY, USA, 1382–1399. doi:10.1145/3676641.3716281
- [33] Nazim Altar Koca, Anh Tuan Do, and Chip-Hong Chang. 2023. Hardware-efficient Softmax Approximation for Self-Attention Networks. In *2023 IEEE International Symposium on Circuits and Systems (ISCAS)*. 1–5. doi:10.1109/ISCAS46773.2023.10181465
- [34] Alexander Kolesnikov, Alexey Dosovitskiy, Dirk Weissenborn, Georg Heigold, Jakob Uszkoreit, Lucas Beyer, Matthias Minderer, Mostafa Dehghani, Neil Houlsby, Sylvain Gelly, Thomas Unterthiner, and Xiaoohua Zhai. 2021. An Image is Worth 16x16 Words: Transformers for Image Recognition at Scale.
- [35] Kung. 1982. Why systolic architectures? *Computer* 15, 1 (1982), 37–46. doi:10.1109/MC.1982.1653825
- [36] Nandeeeka Nayak, Toluwanimi O. Odemuyiwa, Shubham Ugare, Christopher W. Fletcher, Michael Pellauer, and Joel S. Emer. 2023. TeAAL: A Declarative Framework for Modeling Sparse Tensor Accelerators. In *2023 56th IEEE/ACM International Symposium on Microarchitecture (MICRO)*. IEEE Computer Society, Los Alamitos, CA, USA, 1255–1270. <https://doi.ieeecomputersociety.org/>
- [37] Nandeeeka Nayak, Xinrui Wu, Toluwanimi O. Odemuyiwa, Michael Pellauer, Joel S. Emer, and Christopher W. Fletcher. 2024. FuseMax: Leveraging Extended Einsums to Optimize Attention Accelerator Design. In *2024 57th IEEE/ACM International Symposium on Microarchitecture (MICRO)*. 1458–1473. doi:10.1109/MICRO61859.2024.00107
- [38] Long Ouyang, Jeff Wu, Xu Jiang, Diogo Almeida, Carroll L. Wainwright, Pamela Mishkin, Chong Zhang, Sandhini Agarwal, Katarina Slama, Alex Ray, John Schulman, Jacob Hilton, Fraser Kelton, Luke Miller, Maddie Simens, Amanda Askell, Peter Welinder, Paul Christiano, Jan Leike, and Ryan Lowe. 2022. Training language models to follow instructions with human feedback. arXiv:2203.02155 [cs.CL] <https://arxiv.org/abs/2203.02155>
- [39] Adam Paszke, Sam Gross, Francisco Massa, Adam Lerer, James Bradbury, Gregory Chanan, Trevor Killeen, Zeming Lin, Natalia Gimelshein, Luca Antiga, Alban Desmaison, Andreas Köpf, Edward Yang, Zach DeVito, Martin Raison, Alykhan Tejani, Sasank Chilamkurthy, Benoit Steiner, Lu Fang, Junjie Bai, and Soumith Chintala. 2019. *PyTorch: an imperative style, high-performance deep learning library*. Curran Associates Inc., Red Hook, NY, USA.
- [40] Pratyush Patel, Esha Choukse, Chaojie Zhang, Aashaka Shah, Íñigo Goiri, Saeed Maleki, and Ricardo Bianchini. 2024. Splitwise: Efficient Generative LLM Inference Using Phase Splitting. In *2024 ACM/IEEE 51st Annual International Symposium on Computer Architecture (ISCA)*. 118–132. doi:10.1109/ISCA59077.2024.00019
- [41] Paul Rosenfeld, Elliott Cooper-Balis, and Bruce Jacob. 2011. DRAM-Sim2: A Cycle Accurate Memory System Simulator. *IEEE Computer Architecture Letters* 10, 1 (2011), 16–19. doi:10.1109/L-CA.2011.4
- [42] Jay Shah, Ganesh Bikshandi, Ying Zhang, Vijay Thakkar, Pradeep Ramani, and Tri Dao. 2024. FlashAttention-3: Fast and Accurate Attention with Asynchrony and Low-precision. arXiv:2407.08608 [cs.LG] <https://arxiv.org/abs/2407.08608>
- [43] Antonio G.M. Strollo, Davide De Caro, and Nicola Petra. 2011. Elementary Functions Hardware Implementation Using Constrained Piecewise-Polynomial Approximations. *IEEE Trans. Comput.* 60, 3 (2011), 418–432. doi:10.1109/TC.2010.127
- [44] Emma Strubell, Ananya Ganesh, and Andrew McCallum. 2019. Energy and Policy Considerations for Deep Learning in NLP. *ArXiv abs/1906.02243* (2019). <https://api.semanticscholar.org/CorpusID:174802812>
- [45] Ashish Vaswani, Noam Shazeer, Niki Parmar, Jakob Uszkoreit, Llion Jones, Aidan N. Gomez, Lukasz Kaiser, and Illia Polosukhin. 2017. Attention is all you need. In *Proceedings of the 31st International Conference on Neural Information Processing Systems* (Long Beach, California, USA) (NIPS'17). Curran Associates Inc., Red Hook, NY, USA, 6000–6010.
- [46] Zhican Wang, Gang Wang, and Guanghui He. 2025. COSA Plus: Enhanced Co-Operative Systolic Arrays for Attention Mechanism in Transformers. *IEEE Transactions on Computer-Aided Design of Integrated Circuits and Systems* 44, 2 (2025), 723–736. doi:10.1109/TCAD.2024.3434447
- [47] Zhican Wang, Gang Wang, Honglan Jiang, Ningyi Xu, and Guanghui He. 2023. COSA:Co-Operative Systolic Arrays for Multi-head Attention Mechanism in Neural Network using Hybrid Data Reuse and Fusion Methodologies. In *2023 60th ACM/IEEE Design Automation Conference (DAC)*. 1–6. doi:10.1109/DAC56929.2023.10247678
- [48] C. Wilson. 2024. Verilator: The fastest free Verilog HDL simulator. <https://verilator.org/>. Version 5.024.
- [49] Jianxing Xu, Yuanbo Wen, Zikang Liu, Ruibai Xu, Tingfeng Ruan, Jun Bi, Rui Zhang, Di Huang, Xinkai Song, Yifan Hao, Xing Hu, Zidong Du, Chongqing Zhao, Jiang Jie, and Qi Guo. 2025. Mosaic: Exploiting Instruction-Level Parallelism on Deep Learning Accelerators with iTex Tessellation. In *Proceedings of the 30th ACM International Conference on Architectural Support for Programming Languages and Operating Systems, Volume 2* (Rotterdam, Netherlands) (ASPLOS '25). Association for Computing Machinery, New York, NY, USA, 672–688. doi:10.1145/3676641.3716262